BJRS
BRAZILIAN JOURNAL OF RADIATION SCIENCES

doi.org/10.15392/2319-0612.2024.2487
2024, 12(3) | 01-21 | e2487
Submitted: 2024-05-16
Accepted: 2024-08-21

Effects of PET image reconstruction parameters and tumor-to-background uptake ratio on quantification of PET images from PET/MRI and PET/CT systems

Ali Hussain, A.[a]; Forssell-Aronsson, E.[a,b]; Rosholm, T.[b]; Mehrara, E. [a,b*]

[a] Dept of Medical Radiation Sciences, Institute of Clinical Sciences, Sahlgrenska Academy, University of Gothenburg, Gothenburg, Sweden

[b] Medical Physics and Biomedical Engineering, Sahlgrenska University Hospital, Gothenburg, Sweden.

*Correspondence: e.mehrara@radfys.gu.se

Abstract: Introduction: PET/CT and PET/MRI are valuable multimodality imaging techniques for visualizing both functional and anatomical information. The most used PET reconstruction algorithm is Ordered Subset Expectation Maximization (OSEM). In OSEM, the image noise increases with increased number of iterations, and the reconstruction needs to be stopped before complete convergence. The Bayesian penalized likelihood (BPL) algorithm, recently introduced, uses a noise penalty factor (β) to achieve full convergence while controlling noise. This study aims to evaluate how reconstruction algorithms and lesion radioactivity levels affect PET image quality and quantitative accuracy across three different PET systems. Materials and Methods: A NEMA phantom was filled with 18F and scanned by one PET/MRI and two PET/CT systems with sphere-to-background concentration ratio (SBR) of 2:1, 4:1, or 10:1. PET images were reconstructed with OSEM or BPL with TOF. The number of iterations and β-values were varied, while the matrix size, number of subsets, and filter size remained constant. Contrast recovery (CR) and background variability (BV) were measured in images. Results: CR increased with increased sphere size and SBR. CR and BV decreased with increased β for the 10mm sphere. Increased number of iterations in OSEM showed increased BV with limited variation in CR. BPL gave higher CR and lower BV values than OSEM. The optimal reconstruction was BPL with β between 150 and 350, where BPL was available, and OSEM with two iterations and 21 subsets for the PET/CT without BPL. Conclusion: BPL outperforms OSEM, and SBR significantly influences tracer uptake quantification in small lesions. Future studies should explore the clinical implications of these findings on diagnosis, staging, prognosis, and treatment follow-up.

Keywords: OSEM, BPL, NEMA, Q-clear.

BJRS
BRAZILIAN JOURNAL OF RADIATION SCIENCES

doi.org/10.15392/2319-0612.2024.2487
2024, 12(3) | 01-21 | e2487
Submitted: 2024-05-16
Accepted: 2024-08-21

Efectos de los parámetros de reconstrucción de imágenes PET y la relación de captación tumor-fondo en la cuantificación de imágenes PET de los sistemas PET/MRI y PET/CT

Resumen: Introducción: El PET/CT y PET/MRI son técnicas valiosas de imagen multimodal para la visualización de información tanto funcional como anatómica. El algoritmo de reconstrucción para PET más utilizado es la maximización de expectativas de subconjuntos ordenados (OSEM). En OSEM, el ruido de la imagen aumenta con el número de iteraciones, y la reconstrucción debe detenerse antes de la convergencia completa. El algoritmo de reconstrucción de probabilidad penalizada bayesiano (BPL), introducido recientemente, utiliza un factor de penalización de ruido (β) para lograr una convergencia completa mientras controla el ruido. Este estudio tiene como objetivo evaluar cómo los algoritmos de reconstrucción y los niveles de radiación de las lesiones afectan la calidad de la imagen PET y la precisión cuantitativa en tres sistemas PET diferentes. Materiales y Métodos: Se llenó un fantoma NEMA con 18F y se escaneó con un sistema PET/MRI y dos sistemas PET/CT con una relación de concentración esfera/fondo (SBR) de 2:1, 4:1 o 10:1. Las imágenes PET se reconstruyeron con OSEM o BPL con TOF. Se varió el número de iteraciones y los valores de β, mientras que el tamaño de la matriz, el número de subconjuntos y el tamaño del filtro permanecieron constantes. Se midieron la recuperación de contraste (CR) y la variabilidad del fondo (BV) en las imágenes. Resultados: CR aumentó con el tamaño de la esfera y SBR. CR y BV disminuyeron con un aumento de β para la esfera de 10 mm. Un mayor número de iteraciones en OSEM mostró un aumento de BV con variación limitada en CR. BPL mostró valores más altos de CR y más bajos de BV que OSEM. La reconstrucción óptima fue BPL con β entre 150 y 350, donde BPL estaba disponible, y OSEM con dos iteraciones y 21 subconjuntos para el PET/CT sin BPL. Conclusión: BPL supera a OSEM y SBR influye significativamente en la cuantificación de la captación del trazador en lesiones pequeñas. Estudios futuros deberán explorar las implicaciones clínicas de estos hallazgos en el diagnóstico, la estadificación, el pronóstico y el seguimiento del tratamiento.

Palabras-clave: OSEM, BPL, NEMA, Q-clear.

SBPR

1. INTRODUCTION

Positron emission tomography (PET) is a functional imaging technique that enables non-invasive quantitative measurement of biological processes in vivo, and it is one of the most important cancer imaging tools. PET imaging is usually integrated with other modalities, including computed tomography (CT) or magnetic resonance imaging (MRI). The purpose of the combination is to produce medical images with different functional and anatomical information simultaneously. This information makes it possible to provide more accurate diagnosis, staging, and restaging, especially for the management of cancer patients. The most used PET tracer is ^{18}F-fluorodeoxyglucose (^{18}F-FDG), which provides information on glucose uptake and glycolysis rate. FDG accumulates to a higher extent in malignant cells than in normal cells and illustrates metabolic abnormalities before morphological changes can be visualized. Standardized uptake value (SUV) is a semi-quantitative measure for tumor uptake and is used as a parameter to assess tumor response to treatment [1]. Therefore, any imaging parameter that affects the quantification of radioactivity uptake in tumors may, in turn, affect the estimation of SUV.

PET images are computationally reconstructed from raw data, and there are limitations in detecting small lesions due to relatively low signal-to-noise ratio (SNR) and limited spatial resolution. Although there have been several technical developments in PET technology in recent decades, e.g., TOF acquisition and advanced image reconstruction methods [2, 3], the reconstruction parameters play an important role in image quality and quantification.

The reconstruction algorithms in PET are based on iterative methods, and the most commonly used algorithm is Ordered Subset Expectation Maximization (OSEM). OSEM is an accelerated reconstruction method that allows modelling of various system factors in the process, including TOF and correction for point spread function (PSF) [3]. PSF-correction in

PET images improves spatial resolution, minimizes partial volume effects, and increases SNR in PET images, but it can alter quantitative accuracy. Nevertheless, TOF and PSF-correction have shown to improve lesion detectability and SUV-quantification in small lesions [4].

The biggest disadvantage of OSEM reconstruction is the trade-off between the number of subsets and iterations and image quality. OSEM divides the projections into subsets that are analyzed sequentially during each iteration. When the number of subsets increases, noise and artifacts may increase. The problem appears because the subset contains a small amount of tomographic and statistical information. An increased number of iterations also leads to increased noise, reducing accuracy and image quality. Thus, the OSEM algorithm is often stopped before complete convergence will be achieved [5, 6].

Bayesian penalized likelihood (BPL) is a PET image reconstruction algorithm that uses a noise penalty factor (β) to suppress image noise. GE Healthcare has introduced BPL (called Q-clear) in new PET/CT and PET/MRI systems. The penalty factor is a function of the difference in values between adjacent voxels and their sum, and changing the β-value can change the noise suppression level. Unlike the conventional OSEM algorithm, an increased number of iterations in the BPL algorithm does not increase noise, and effective convergence can be achieved with more iterations. BPL has been shown to significantly improve SNR in clinical PET scans especially for small lesions [7]. High β-values result in stronger noise suppression, but, on the other hand, they can affect other factors such as edge detection, volume determination and SUV. The optimal β-values in clinical practice are necessary to estimate with a balance between the calculated statistics and the resulting image quality [6].

Quantification of tumor uptake in PET images depends on the choice of reconstruction algorithms/parameters and the PET system used for imaging. The aim of this study was to analyze the effect of reconstruction parameters, tumor size, and tumor-to-background (T/B) uptake ratio on the measured SUV in one PET/MRI and two PET/CT systems.

2. MATERIALS AND METHODS

2.1. Phantom preparation

The National Electrical Manufacturers Association (NEMA) image quality phantom is commonly used for assessing the performance of the PET component of hybrid imaging systems, including PET/CT and PET/MR [8]. One of the measures of PET image quality is image contrast, which reflects the differences in pixel intensities between various radioactive concentration levels [9]. Contrast recovery (CR) and background variability (BV) can be analyzed with the NEMA phantom, where CR is the ratio between measured and true concentrations in a region-of-interest (ROI), and BV indicates the noise level of the image, so a higher BV reflects a higher level of image noise. CR and BV are used to investigate the impact of various reconstruction algorithms and parameters on reconstructed images.

A NEMA IEC body phantom (Data Spectrum, Durham, North Carolina, USA) was used to collect data in this study. The phantom contains six fillable spheres with internal diameters of 10, 13, 17, 22, 28 and 37 mm, respectively, which are regarded as tumors in the present study.The phantom also includes plastic-filled material with a low atomic number to represent the lungs (with an average density of 0.3 g/ml), centered inside the phantom body and extending axially through the entire phantom.

The sphere-to-background activity concentration ratios (SBR) were chosen based on data from previously published patient PET/CT studies using ^{68}Ga-PSMA and ^{18}F-FDG [10-13]. Table 1 shows an overview of tumor-to-background activity concentration ratios (T/B) for different tumors from clinical PET/CT studies. The following procedure was used to fill the phantom background and spheres with homogeneous solutions of ^{18}F-FDG to obtain SBR values of 2:1, 4:1, and 10:1. Detailed values of specific activities for spheres and the background of the phantom can be found in Table 2.

Table 1: Tumor-to-background, (T/B) values from 18F-FDG and 68Ga-PSMA imaging of patients.

Reference	Tracer	T/B Mean (SD)	T/B Median (range)
Glioma brain tumors [10]	18F-FDG	1.3 (0.4)	-
Positive cardiac lesions [11]	18F-FDG	4.5 (1.5)	-
Primary tumors [12]	68Ga-PSMA-11	-	19 (6.7 – 92)
Positive axillary lymph nodes [13]	18F-FDG	4.5 (2.0)	-
Bone metastases [12]	68Ga-PSMA-11	-	7.8 (1.5 – 35)

The phantom preparation started by filling the phantom background with 50%, 25%, or 10 % of the total phantom volume with water. A precise measuring volumetric flask was used to scale water volume. A PET Infusion System (MEDRAD Intego, Bayer Healthcare, USA) was used to fill the phantom background with 49 MBq (for SBR 2:1 and 4:1) or 20 MBq (for SBR 10:1) at scan time. The solution in the phantom was shaken carefully to obtain homogeneity. The spheres where then filled with the background solution using a syringe with a long needle and the remaining solution in the syringe was returned to the phantom background. The two largest spheres (with 28 mm and 37 mm diameters) were filled with nonradioactive water. The background region was then fully filled up with water.

2.2. Image acquisition

Data acquisition was performed using three different cameras: PET/CT-1 (Discovery MI, GE Healthcare, Chicago, Illinois, USA), PET/CT-2 (Biograph mCT, Siemens Healthineers AG, Erlangen, Germany), and PET/MRI (Signa 3T, GE Healthcare, Chicago, Illinois, USA). The filled NEMA phantom was placed on the patient table and the landmark was aligned with the central plane of spheres.

The scan was performed following the vendor's instructions, where a pre-loaded attenuation-map template is automatically aligned with the scanned phantom data using a three-minute positioning scan. The prepositioning scan was then followed by a PET scan with varying acquisition times depending on the SBR at the beginning of the scan. Table 2

shows the acquisition time, ^{18}F-FDG activity concentration of spheres (AC_S), and the phantom background (AC_B) at the start of acquisition. All emission data were acquired in list mode in order to be able to reconstruct the data afterwards.

Data acquisitions procedures with GE and Siemens PET/CT systems were similar. First, an initial x-ray transmission scout image was acquired and used to define the axial field of the CT and PET scans, followed by an attenuation correction CT (ACCT) scan. Immediately after the ACCT scan, the PET scan was performed with acquisition times presented in Table 2. The slice thickness was 1.5 mm and 2.78 mm for the Siemens and GE systems, respectively. All PET/CT emission data were acquired in list mode.

Table 2: ^{18}F concentrations in phantom spheres (AC_S) and background (AC_B), together with acquisition times used for different sphere-to-background ratios (SBR) for image acquisition at PET/CT-1, PET/CT-2, and PET/MRI systems. ^{18}F-FDG activity concentrations are given at the start of acquisition.

System	SBR	AC_S (kBq/ml)	AC_B (kBq/ml)	Acquisition time (min)
PET/CT-1: GE Discovery MI	2:1	4.7	2.4	40
PET/CT-1: GE Discovery MI	4:1	15	3.9	15
PET/CT-1: GE Discovery MI	10:1	18	1.8	25
PET/CT-2: Siemens Biograph mCT	2:1	9.9	4.9	20
PET/CT-2: Siemens Biograph mCT	4:1	18	4.7	10
PET/CT-2: Siemens Biograph mCT	10:1	11	1.1	30
PET/MRI: GE Signa	2:1	7.2	3.6	23
PET/MRI: GE Signa	4:1	23	5.7	10
PET/MRI: GE Signa	10:1	7.3	0.73	60

PET images were reconstructed using OSEM with TOF, 21 subsets, and 2, 3, 4, 6, and 8 iterations for the Siemens PET/CT system. For GE PET/CT and PET/MRI systems, the PET images were reconstructed using OSEM with TOF, 16 subsets, and 3, 4, 6, 8, and 10 iterations as well as BPL (Q-Clear) with TOF and β-values of 100, 150, 350, 550, 750, and 1000. Images were reconstructed with one parameter varied at a time, while the other

parameters were kept constant. The matrix size was 256x256, and the filter size was set to a full-width-at-half-maximum (FWHM) of 5 mm for all reconstructions.

2.3. Data analysis

Vendor-provided NEMA analysis tools for each system were used for measuring the contrast recovery (CR) and background variability (BV) in NEMA phantom images. For GE PET/CT, the SPARC standalone PET reconstruction server (GE Healthcare, Chicago, Illinois, USA) was used. The analysis tools automatically positioned the regions of interest (ROI) over each sphere and in the background area of the reconstructed PET images (Figure 1) and calculated the CR and BV values.

Figure 1. ROI delineation for calculation of contrast recovery, CR, and background variability, BV, in NEMA phantom images. Left: Siemens PET/CT. Right: GE PET/CT (similar to GE PET/MRI).

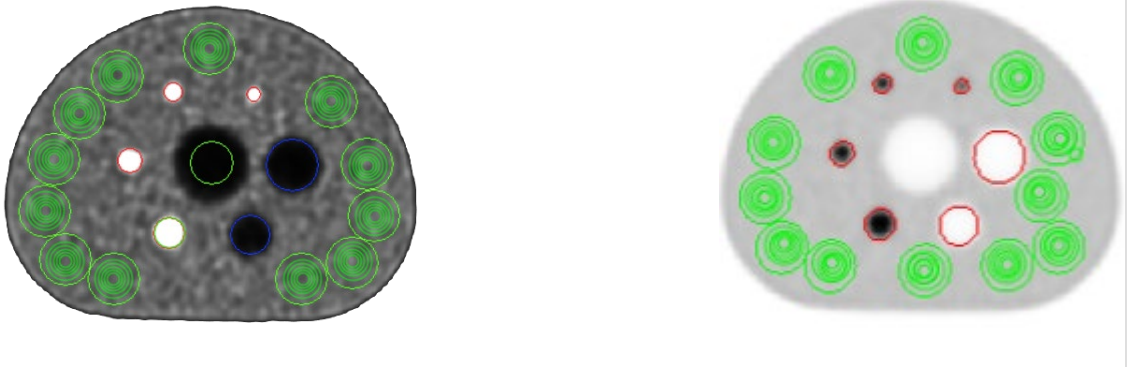

CR and BV were determined based on the number of counts in the ROI and the activity in each sphere of interest. The CR of each sphere (CR_S) is calculated by the following equation:

$$CR_S = \frac{\frac{C_S}{C_B} - 1}{\frac{AC_S}{AC_B} - 1} \times 100\%,$$

where C_S is the average number of counts in the ROI in the transverse image slice containing the sphere and C_B is the average number of counts in the twelve background ROIs. The diameter of the background ROI is the same size as the sphere, as illustrated in Figure 1.

AC_S/AC_B is the actual radioactivity-concentration ratio between the sphere and the background volume. The BV in each image is calculated by following equation:

$$BV = \frac{SD}{C_B} \times 100\%,$$

where SD is the standard deviation of the number of counts in the background ROI for the sphere. Excel was used for statistical analysis, and the significance level was 0.05.

3. RESULTS AND DISCUSSIONS

3.1. Contrast recovery for OSEM reconstruction

The result of the reconstruction using the OSEM algorithm for PET images from all three systems is illustrated in Figure 2. The results show a trend of increased CR with increased sphere size and SBR for all PET systems. In addition, a trend of increased CR with an increased number of iterations (n) was observed, which was substantial for lower SBR (2:1 and 4:1) and smaller sphere sizes (10mm and 13mm). The largest increase of CR with n was observed for the 10mm sphere and was highest for the Biograph mCT and SBR 2:1 with an increase of 52% from two to eight iterations.

3.2. Contrast recovery for BPL (Q-clear) reconstruction

Figure 3 shows the CR of spheres from PET images obtained with PET/CT-1 and PET/MRI systems with varying SBR and β-values. All plots show a similar trend: CR decreased with increased β-value and increased sphere size. The results showed an increase in CR by more than 100 %, with an increase in SBR from 2:1 to 10:1, in the smallest sphere, i.e., 10 mm. The most significant CR decrease with increased β-value occurred for the 10 mm and 13 mm spheres.

Figure 2. Contrast recovery (CR) for a varying number of iterations (2-10) in OSEM algorithm as a function of sphere diameter for different SBR and PET system. A-C) PET/CT-1. D-F) PET/MRI. G-I) PET/CT-2. All reconstructions were made with a constant matrix size of 256x256 and a 5 mm FWHM Gaussian filter.

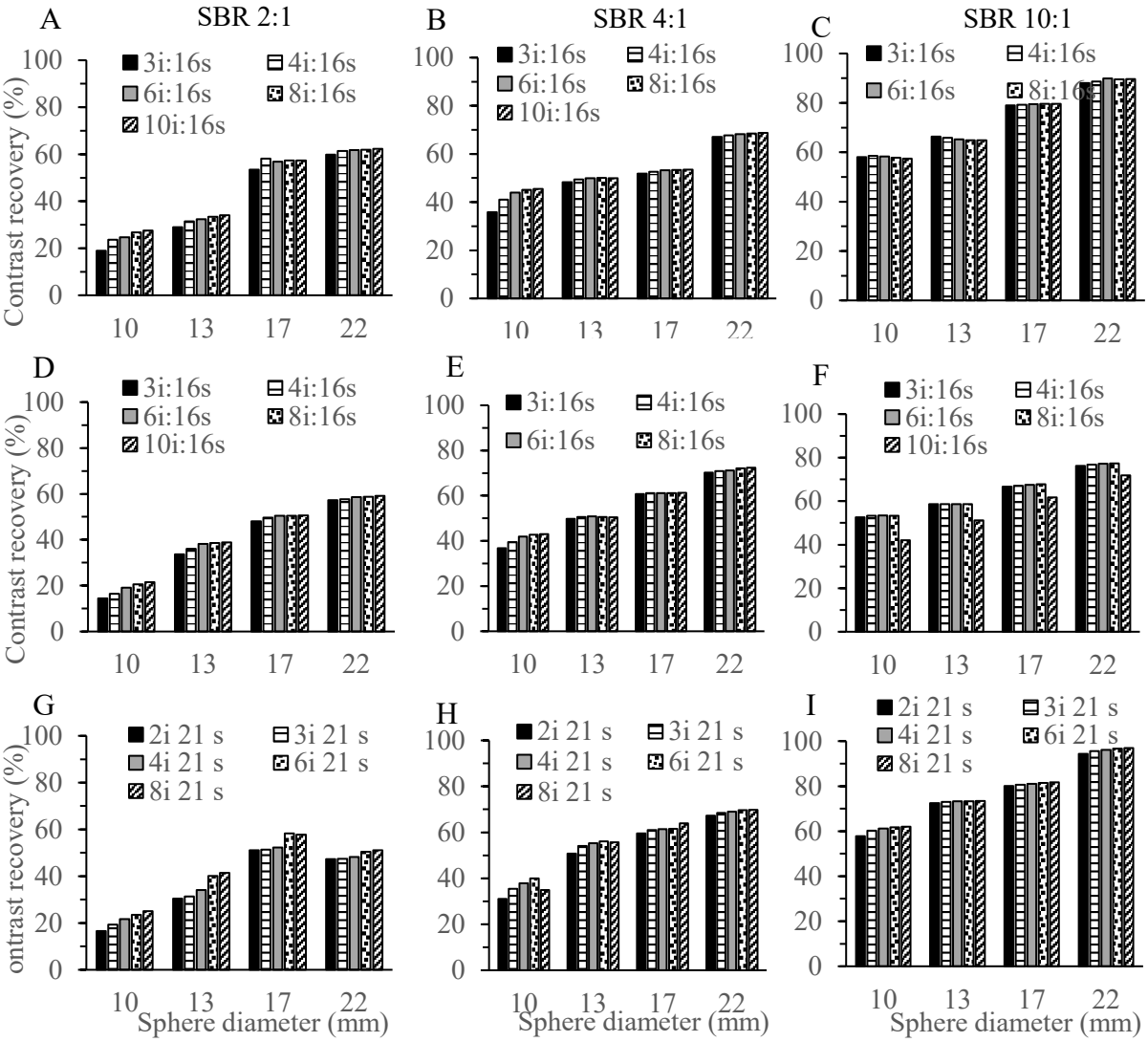

Figure 3. Contrast recovery (CR) for varying β-value in BPL algorithm as a function of sphere diameter for different SBR and PET system. **A-C**) PET/CT-1. **D-F**) PET/MRI. All reconstructions were made with a constant matrix size of 256x256 and a 5 mm FWHM Gaussian filter.

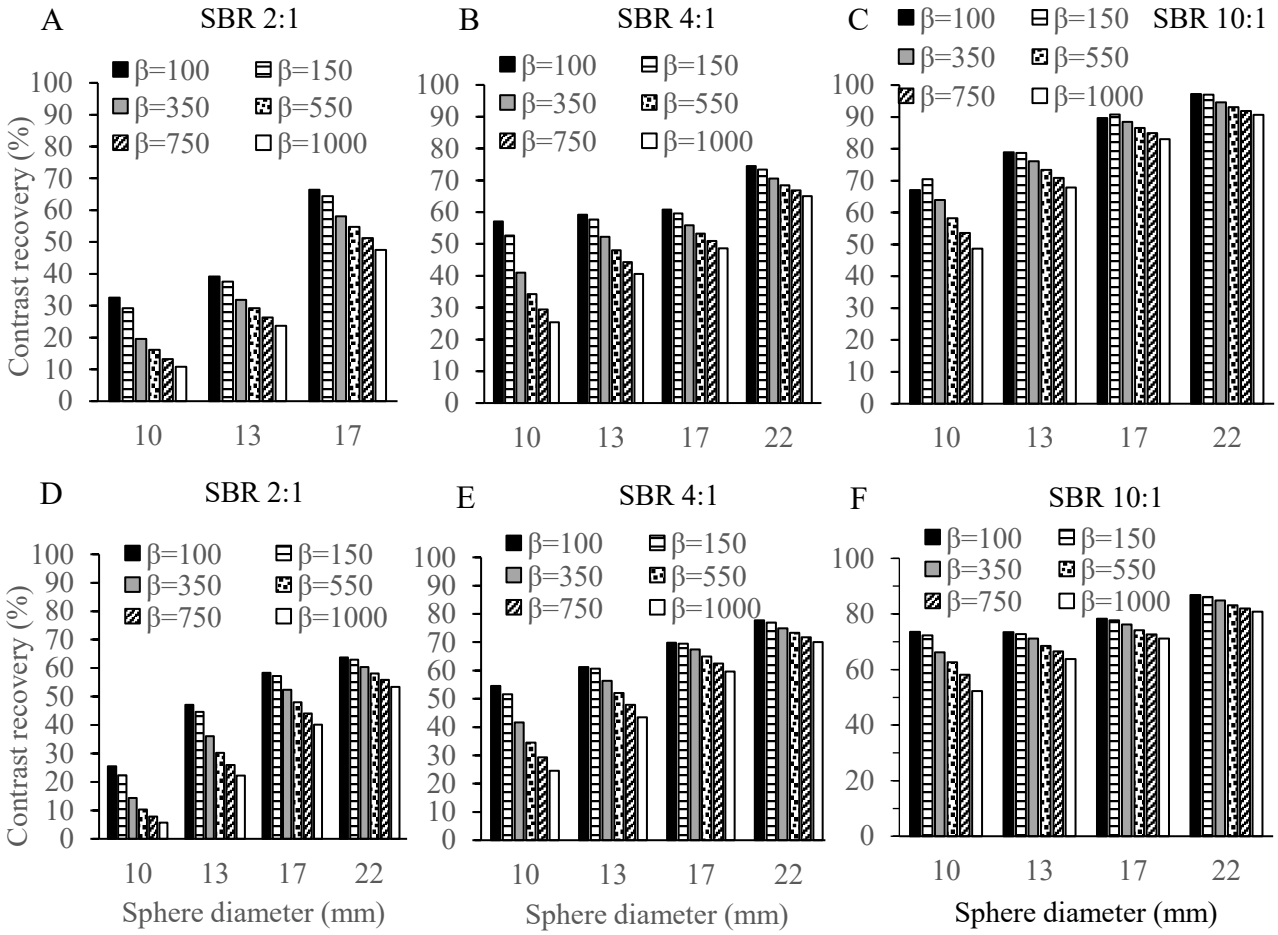

3.3. Contrast recovery versus background variability

The effects of changing the reconstruction parameters in OSEM and Q-clear reconstruction algorithm were investigated to evaluate how this would impact the quantification of radioactivity concentration in spheres and image noise. In this study, the 10 mm sphere was chosen for further analysis due to the highest variation observed between different reconstructions.

3.4. Contrast recovery versus background variability for OSEM reconstruction

The relation between CR and BV for the 10 mm sphere using different OSEM and BPL reconstructions with TOF is shown in Figure 4 for different SBRs. In general, BV increased with an increased number of iterations for all SBR values and camera systems. For SBR 2:1, however, the increase was not significant for PET/CT-1 compared to PET/CT-2 and PET/MRI, and even other SBR values. PET/CT-2 showed the highest BV for all activity ratios compared to the other systems, and the same result was obtained for all sphere sizes. This high BV can affect the visibility of spheres in the reconstructed image. For SBR 10:1, BV increased with the number of iterations, while CR remained almost constant.

The optimum number of iterations should reduce image noise without compromising quantification. For imaging ROI with high activity concentrations, reconstruction should be performed with a low number of iterations such as three iterations and 16 subsets for PETCT-1 and PET/MRI and two iterations and 21 subsets for PET/CT-2, in order to achieve the best image quality with acceptable BV. Furthermore, SBR 2:1 did not show a large increase of BV with an increased number of iterations. It would be more suitable to use a higher number of iterations to obtain the best contrast in the image as possible in regions of low activity concentration. SBR 4:1 data showed an increase in CR and BV with the number of iterations, so it would be best to find a trade-off between BV and CR by analyzing the image, but six iterations can be a good choice.

3.5. Contrast recovery versus background variability for Q-Clear reconstruction

Figure 4 demonstrates CR as a function of BV for the Q-clear reconstruction algorithm with varying β-values from 100 to 1000. The results show that the CR and BV increased when the β-value decreased. With lower β-values, the image noise increased. A higher SBR resulted in a higher CR value. The comparison between PET systems showed that PET images from PET/CT-1 gave higher CR and lower BV values than PET/MRI. Higher BV values were observed in 13, 17, and 22mm spheres with an increased sphere size

for PET images on the PET/MRI system. For 22 mm spheres, the PET/CT-1 showed a small increase in CR with varying β-values. For the 10 mm sphere, there was a significant difference ($P<0.05$) in CR and BV values obtained by different SBR with different β-values.

Figure 4. Contrast recovery versus background variability for 10 mm sphere, matrix 256x256, 5 mm FWHM Gaussian filter. **Left**: OSEM + TOF. Number of iterations left to right : 3i, 4i, 6i, 8i, 10i for PET/CT-1 and PET/MRI and 2i, 3i, 4i, 6i, 8i for PET/CT-2 for respective SBR (2:1, 4:1, 10:1). Subsets for all reconstructions : 16s for PET/CT-1 and PET/MRI and 21s for PET/CT-2. **Right**: BPL (Q-Clear) reconstruction + TOF. The markers represent β-values of 100, 150, 350, 550, 750, and 1000 from right to left, respectively. Note: While this figure illustrates the results for the 10 mm sphere due to its significant partial volume effects, similar trends were observed for spheres of 13, 17, and 22 mm diameters, with differences being less pronounced as sphere size increases.

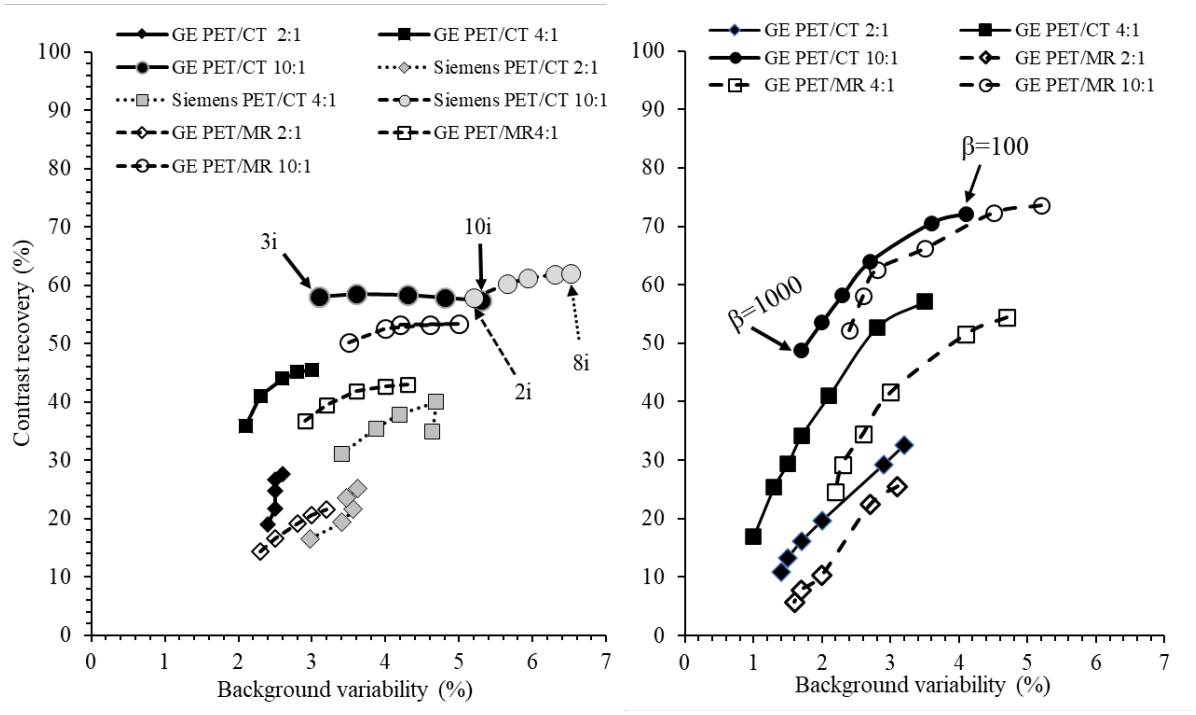

A β-value higher than 750 showed to reduce the quantitative accuracy due to the low CR level. The optimum β-value to use for the quantification of 10 mm sphere should be in the range of 150-350 for both PET/CT-1 and PET/MRI systems and applies especially for 4:1 and 10:1 SBRs. For lower SBR values, such as 2:1, a low β-value gives more accurate CR without high noise in the image.

3.6. Quantitative comparison between OSEM and Q-clear reconstruction

Figure 5 illustrates the contrast recovery ratio between Q-clear and OSEM reconstructions for different SBR values. The β-value was 150 for SBR 2:1 and 350 for SBR 4:1 for both cameras. For SBR 10:1, the β-value was 150 for PET/CT-1 and 350 for PET/MRI. The OSEM parameters were three iterations and 16 subsets for all plots. The ratio reduced with sphere size, and there was less than a 5% difference in value between PET/CT-1 and PET/MRI systems for all sphere sizes. The ratio was higher than one in all results, and there was a statistically significant difference in CR between OSEM and the Q-clear algorithms ($P<0.05$). This means that there was always an improvement in image quantification with Q-clear.

Figure 5. CR(Q-clear)/CR(OSEM) as a function of sphere size for SBR 2:1, 4:1 and 10:1. β-value was 150 or 350 and OSEM parameters were three iteration and 16 subsets for both cameras. Both reconstructions were made with constant matrix size (256x256) and Gaussian filter (5 mm). CR: Contrast recovery

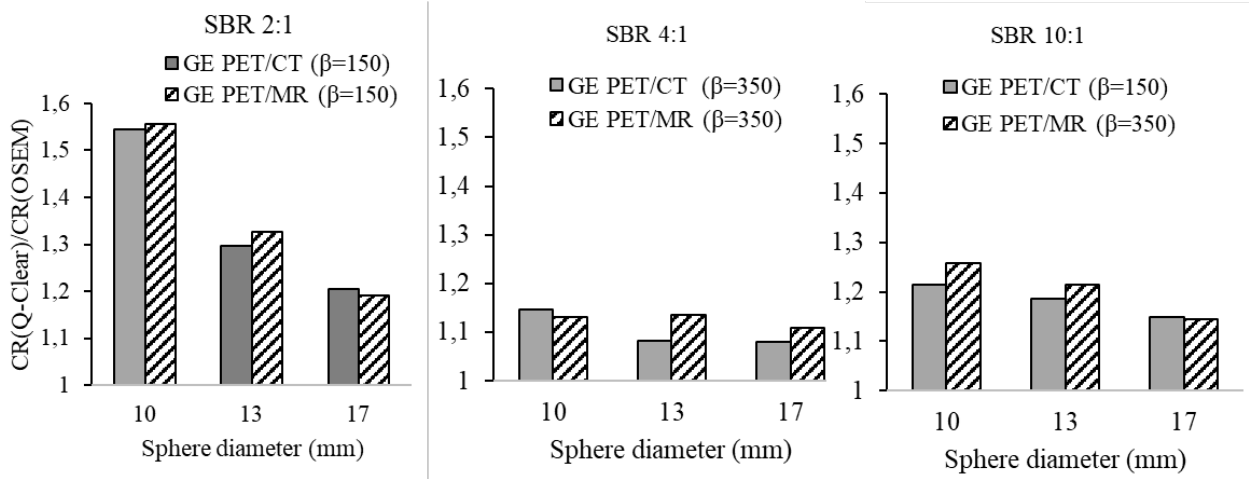

PET/MRI and PET/CT multimodality imaging systems are valuable tools in clinical oncologic imaging due to the ability to combine functional and structural information using a single device and during a single imaging session. However, the quantification of tumor uptake, e.g. SUV, and the image noise level depend on lesion size and the radioactivity concentration in lesion compared to surrounding tissue. In this study, PET images from PET/MRI, PET/CT-1, and PET/CT-2systems were analyzed using the NEMA phantom, which is the standard method to assess the performance of the PET systems. The PET image noise and quantification accuracy for different SBR levels were investigated by measuring CR and BV in images obtained with different reconstruction algorithms and parameters.

The results showed that CR increased with increasing sphere size in all images. Ideally, CR should be 100%, but the partial volume effect in PET images can result in an underestimation of radioactivity (uptake) in the ROI of spheres (lesions) due to spill-out effect [8]. The effect becomes more important as the sphere size decreases. Another trend that was observed was that CR decreased with increasing β-value (in BPL) and increasing number of iterations (in OSEM) for all SBR values and camera systems. CR was higher for the PET/CT-1 compared to the PET/MRI system. BV decreased with increased β-value for both cameras, where BV reflects the noise level of the image. In OSEM reconstruction, CR reached a plateau for SBR 10:1 with increased number of iterations, while BV increased.

The results demonstrated that Q-clear with TOF using a β-value between 150 and 350 for GE PET/MRI and PET/CT is an appropriate choice for Q-clear reconstruction. β-values were then chosen as a trade-off between contrast improvement and remaining at the same noise level as OSEM. The optimal OSEM reconstruction was for PET/CT-1 and PET/MRI systems with TOF information using three iterations, 16 subsets, and 5 mm FWHM Gaussian filter, and for PET/CT-2 system, two iterations, 21 subsets, and 5 mm FWHM Gaussian filter.

The optimal reconstruction algorithms and parameters cannot be directly applied to clinical imaging, because the present study was based on NEMA phantom. Further studies are needed to examine how clinical PET images should be analyzed, including choice of reconstruction algorithm, parameters, and the T/B ratio.

A previous study based on a NEMA phantom experiment compared Q-clear reconstruction parameters with OSEM reconstruction with three iterations, 16 subsets, and a Gaussian post-filter with FWHM of 5.0 mm [14]. The results of that study suggested that the optimal β-value depends on the contrast and the lesion's size. A high β-value can lead to a negative impact on the detectability of the small lesion. It was then suggested that β-values ranging between 300 and 400 will maximize the CR and contrast-to-noise ratio (CNR) for small spheres. This β-value range from that study is similar to the results from the present study, where we found that the best trade-off between CR and BV was achieved with a β-value of 350 for SBR 10:1 and SBR 4:1. Another study evaluated and compared PET image reconstruction algorithms on image quality and quantitative parameters in patients with initial lung cancer using a PET/CT scanner [15]. Those results showed an increased image quality, image sharpness, and tumor lesion conspicuity with Q-clear compared to OSEM. It was even suggested to adjust β-values to the injected ^{18}F-FDG activity to provide more patient-tailored PET imaging and for maintaining image quality, while reducing the absorbed dose to the patient. A lower dose is especially highly preferred for young patients. A higher β-value (450 - 600) was suggested to be more appropriate for a patient, who received lower ^{18}F-FDG activity (< 2 MBq/kg) compared with patients who received higher activity (> 2 MBq/kg).

There are previous studies where the performances of different PET/CT and PET/MRI systems have been compared yielding different results in clinical settings. It should be noted that several factors, including detector technology, choice of MR protocol, and timing of the PET acquisition, affect the results of such studies [16-19]. Our results

compare the systems with specified characteristics and show that PET/CT-1 and PET/MRI systems showed better performance than PET/CT-2.

The difference in system technology and reconstruction methods can affect image quality and the quantification of CR for phantom or the SUV for oncological imaging [16]. This effect was shown in two earlier studies that have reported discrepancies in lesion-to-background SUV measured in PET/MRI and PET/CT systems. One of the studies observed significantly lower SUVs for PET data acquired with PET/MRI than for PET/CT for the assessed lesions and different organ systems [16]. In contrast, the other study observed the opposite, where the differences between the systems could even depend on the various time intervals between the two scans. The lesion SUV is in general expected to increase over time [17], due to higher activity concentration differences between tumor and normal tissues [20].

The clinical performance of PET/MRI compared with PET/CT has also been evaluated in mixed cancer patient populations [17, 18, 21, 22]. As expected, PET/CT detected more lesions overall, especially in the lungs. This is due to MRI having lower detectability of small lung lesions, the large thickness of MRI images, and the difference in the performance of the PET scanners. In contrast, PET/MRI had higher diagnostic accuracy performance (+ 13%) than PET/CT for detecting brain and liver metastases due to superior soft-tissue contrast in MRI. Therefore, one of the studies summarized that PET/CT is more likely to be the preferred imaging system for lung and mediastinal nodal disease [17].

Another possible parameter to analyze is CNR for better harmonization of these study results. Then, the detectability between the systems for different reconstruction algorithms and parameters could have been compared. CNR gives information about the visibility of a lesion, while CR gives information on how accurately the system can measure the activity concentration in the lesion. In future studies on clinical images, CNR should also be used, if tumor detectability is evaluated.

In this study, the ROIs were drawn automatically using the NEMA analysis tool of each workstation, which reduced the random uncertainty that can occur by manual positioning. Therefore, there might be a systematic error due to differences between software tools used in different systems. The decrease of CR for 10 and 8 iterations in Fig 2F and 2H, respectively, are probably caused by automatic placement of ROIs. SBR 2:1 results from PET/CT-1 in figure 3 are also missing CR for the 22 mm sphere since the NEMA analysis tool failed to delineate the sphere properly. However, our focus was on smaller sphere sizes, where CR was lower and the effect of SBR on CR are much larger and these deviations do not change the conclusions of this study.

4. CONCLUSIONS

The BPL reconstruction algorithm performed better than OSEM in terms of quantitative measurement of the radioactivity concentration in spheres and image noise. However, the sphere-to-background radioactivity concentration ratio in small spheres is an important factor for the accuracy of quantitative measurements. Future patient studies are recommended to evaluate the effect of the tumor-to-background uptake ratio on the measurement of SUV and its clinical relevance for tumor diagnosis, staging, prognosis, and treatment follow-up.

ACKNOWLEDGMENT

This work was supported by grants from the King Gustav V Jubilee Clinic Cancer Research Foundation (2022:420 and 2021:374), the Swedish state under the agreement between the Swedish government and the county councils – the ALF-agreement (ALFGBG-725031), and Västra Götaland Region, Sweden.

FUNDING

King Gustav V Jubilee Clinic Cancer Research Foundation (2022:420 and 2021:374), the Swedish state under the agreement between the Swedish government and the county councils – the ALF-agreement (ALFGBG-725031), and Västra Götaland Region, Sweden.

CONFLICT OF INTEREST

All authors declare that they have no conflicts of interest.

REFERENCES

[1] Wahl, R.L., et al., From RECIST to PERCIST: Evolving Considerations for PET response criteria in solid tumors. J Nucl Med, 2009. **50 Suppl 1**: p. 122S-50S.

[2] Ziegler, S., et al., NEMA image quality phantom measurements and attenuation correction in integrated PET/MR hybrid imaging. EJNMMI Phys, 2015. **2**(1): p. 18.

[3] Kurita, Y., et al., The value of Bayesian penalized likelihood reconstruction for improving lesion conspicuity of malignant lung tumors on (18)F-FDG PET/CT: comparison with ordered subset expectation maximization reconstruction incorporating time-of-flight model and point spread function correction. Ann Nucl Med, 2020. **34**(4): p. 272-279.

[4] Tsutsui, Y., et al., Edge Artifacts in Point Spread Function-based PET Reconstruction in Relation to Object Size and Reconstruction Parameters. Asia Ocean J Nucl Med Biol, 2017. **5**(2): p. 134-143.

[5] Teoh, E.J., et al., Phantom and Clinical Evaluation of the Bayesian Penalized Likelihood Reconstruction Algorithm Q.Clear on an LYSO PET/CT System. J Nucl Med, 2015. **56**(9): p. 1447-52.

[6] Otani, T., et al., Evaluation and Optimization of a New PET Reconstruction Algorithm, Bayesian Penalized Likelihood Reconstruction, for Lung Cancer Assessment According to Lesion Size. AJR Am J Roentgenol, 2019. **213**(2): p. W50-W56.

[7] Vallot, D., et al., A clinical evaluation of the impact of the Bayesian penalized likelihood reconstruction algorithm on PET FDG metrics. Nucl Med Commun, 2017. **38**(11): p. 979-984.

[8] Association, N.E.M., NEMA Standards Publication NU 2-2007: Performance Measurements of Positron Emission Tomographs. 2007: National Electrical Manufacturers Association.

[9] Cherry, S.R., J.A. Sorenson, and M.E. Phelps, Physics in Nuclear Medicine. 4th ed. 2012, Philadelphia: Elsevier/Saunders.

[10] Kosaka, N., et al., 18F-FDG PET of common enhancing malignant brain tumors. AJR Am J Roentgenol, 2008. **190**(6): p. W365-9.

[11] Liu, Y., Focal mass-like cardiac uptake on oncologic FDG PET/CT: Real lesion or atypical pattern of physiologic uptake? J Nucl Cardiol, 2019. **26**(4): p. 1205-1211.

[12] Rijnsdorp, S., M.J. Roef, and A.J. Arends, Impact of the Noise Penalty Factor on Quantification in Bayesian Penalized Likelihood (Q.Clear) Reconstructions of (68)Ga-PSMA PET/CT Scans. Diagnostics (Basel), 2021. **11**(5).

[13] Straver, M.E., et al., Feasibility of FDG PET/CT to monitor the response of axillary lymph node metastases to neoadjuvant chemotherapy in breast cancer patients. Eur J Nucl Med Mol Imaging, 2010. **37**(6): p. 1069-76.

[14] Caribe, P., et al., Noise reduction using a Bayesian penalized-likelihood reconstruction algorithm on a time-of-flight PET-CT scanner. EJNMMI Phys, 2019. **6**(1): p. 22.

[15] Messerli, M., et al., Impact of a Bayesian penalized likelihood reconstruction algorithm on image quality in novel digital PET/CT: clinical implications for the assessment of lung tumors. EJNMMI Phys, 2018. **5**(1): p. 27.

[16] Drzezga, A., et al., First clinical experience with integrated whole-body PET/MR: comparison to PET/CT in patients with oncologic diagnoses. J Nucl Med, 2012. **53**(6): p. 845-55.

[17] Al-Nabhani, K.Z., et al., Qualitative and quantitative comparison of PET/CT and PET/MR imaging in clinical practice. J Nucl Med, 2014. **55**(1): p. 88-94.

[18] Ishii, S., et al., Comparison of integrated whole-body PET/MR and PET/CT: Is PET/MR alternative to PET/CT in routine clinical oncology? Ann Nucl Med, 2016. **30**(3): p. 225-33.

[19] Oen, S.K., et al., Image quality and detectability in Siemens Biograph PET/MRI and PET/CT systems-a phantom study. EJNMMI Phys, 2019. **6**(1): p. 16.

[20] Baun, C., et al., Quantification of FDG-PET/CT with delayed imaging in patients with newly diagnosed recurrent breast cancer. BMC Med Imaging, 2018. **18**(1): p. 11.

[21] Mayerhoefer, M.E., et al., PET/MRI versus PET/CT in oncology: a prospective single-center study of 330 examinations focusing on implications for patient management and cost considerations. Eur J Nucl Med Mol Imaging, 2020. **47**(1): p. 51-60.

[22] Lee, S.M., et al., Preoperative staging of non-small cell lung cancer: prospective comparison of PET/MR and PET/CT. Eur Radiol, 2016. **26**(11): p. 3850-3857.

LICENSE